Highly Efficient and Stable Cryo-Ground Sulphur Cathode for Li-S batteries

T. Kazda[1,*], M. Krbal[2], M. Pouzar[2,3], J. Vondrák[1], A. Fedorková Straková[4], M. Slávik[5], T. Wagner[2,6], J. M. Macak[2,**]

1 Department of Electrical and Electronic Technology, Faculty of Electrical Engineering and Communication, Brno University of Technology, Technická 10, 616 00 Brno, Czech Republic

2 Center of Materials and Nanotechnologies (CEMNAT), Faculty of Chemical Technology, University of Pardubice, Nam. Cs. Legii 565, 530 02 Pardubice, Czech Republic

3 Institute of Environmental and Chemical Engineering, Faculty of Chemical Technology, University of Pardubice, Studentská 573, 53 210 Pardubice, Czech Republic

4 Department of Physical Chemistry, Faculty of Sciences, P. J. Šafárik University in Košice, Moyzesova 11, SK-04154 Košice, Slovak Republic

5 Graphene Batteries AS c/o Sintef, Forskningsveien 1, 0314 Oslo, Norway

6 Department of General and Inorganic Chemistry, Faculty of Chemical Technology, University of Pardubice, Studentská 573, 53 210 Pardubice, Czech Republic

*Corresponding author, Phone: +420 541 146 177

Postal address: Technická 10, 616 00 Brno, Czech Republic

E-mail address: kazda@feec.vutbr.cz

Fax number: +420 541 146 147

** Corresponding author, Phone + 420 466 037 401, E-mail address: jan.macak@upce.cz

Abstract

Here we report on a Li–S battery with cathode, based on a S powder obtained from bulk amorphous S, by cryogenic grinding. The cathode was prepared from a slurry, wherein the content of cryo-ground S powder was equal to 80 wt. % (corresponds to $\approx$ 2.26 mg cm^{-2}). Other slurry components included carbon Super P, and polyvinylidene fluoride, dispersed in N-methylpyrrolidone. The electrochemical performance of the as-prepared battery was compared to a battery based on an identically prepared paste, but containing reference S powder (with the orthorhombic structure). A longer life cycle, and enhanced capacity per gram, as well as per cm^2 of electrode was revealed for the cryo-ground S-based cathode. The electrochemical results show that the loss in capacity of the cryo-ground S powder cathode was just 3 % after 50 cycles, which suggests on a higher stability of S inside the cathode during cycling.

1. Introduction

The demand for utilization of energy sources for portable devices, electric vehicles, and energy storage systems rapidly increased in the last two decades. As a result, numerous types of batteries have been developed with high capacities and charging rates. [1] Secondary Lithium-Sulphur batteries represent one of the most intriguing battery types being currently developed. [2] The main advantage of the Li-S battery is its very high theoretical capacity of S (1675 mAh g^{-1}) which, in combination with the potential around 2.1 V against Li, means that the theoretical gravimetric energy density exceeds 3000 Wh kg^{-1}. This is a significantly higher value compared to other currently available cathode materials based on $LiCoO_2$, $LiFePO_4$ or $LiNi_{0.33}Mn_{0.33}Co_{0.33}O_2$. [3] [4] Another advantage of S is its abundance, low price and low toxicity. However, several problems have to be solved before commercialization of Li-S batteries. The most serious problem is the shuttle effect - creation of soluble polysulfides (Li_2S_4, Li_2S_6, Li_2S_8) in the electrolyte during cycling. These polysulfides are subsequently deposited on the anode, which leads to a rapid decline of the battery capacity. Additional disadvantages include its low conductivity ($5 \cdot 10^{-30}$ S m^{-1}, resulting from S being an insulator, its low melting point and up to 80% volumetric expansion which leads to the disintegration of electrodes, and further acceleration of the capacity fade. [5] [6] [3] [7] [8] [9] Many researchers have been trying to solve problems related to the shuttle effect and volumetric expansion of S, using encapsulation of S into polymeric or carbon capsules towards an increased stability during cycling. [10] [11] [12] [13] Other possible approaches involve: i) creation of a special layer on the surface of the separator that prevents polysulfides from accessing the anode side [14], ii) creation of special 3D cathode structures into which S is enclosed, thereby preventing deposition of polysulfides at the anode, [7] [9] and, finally, iii) various modifications of the used salts and solvents, including ionic liquids, to reduce the solubility of polysulfides. [7] [15]

In this work, we present an entirely novel approach for the stabilization of the S cathode, which is based on the introduction of amorphous S powder to the cathode slurry, obtained by cryogenic grinding of the amorphous bulk S into particles with irregular shape, and dimensions on the μm scale. We compared the electrochemical performance of the cathode based on the cryo-ground S powder (noted as S_{cryo} cathode) with a cathode based on a reference ball-ground S powder (noted as S_{ref} cathode).

2. Experimental

2.1. Preparation of S powder

The bulk amorphous S was synthesized using the standard melt-quench technique. Pure S pieces (Sigma Aldrich) were placed in a pre-cleaned silica ampoule. The ampoule was evacuated at a pressure of 1×10^{-3} Pa for 30 min and then sealed. Further melting of the S was performed in a rocking furnace with the ampoule exposed to a temperature of 800 °C for 24 h and subsequently quenched into cold water. The cryogenic grinding of as-prepared bulk amorphous S was carried out using the cryogenic impact grinder model 6750 EFM Freezer/Mill (Spex SamplePrep, USA). The grinding procedure was carried out inside polycarbonate vials (model 6751C20 - volume 25 ml) in the presence of liquid N_2. The operating programme consisted of one precooling step (10 min), and six grinding steps (30s), separated from one another by re-cooling periods (60s). The frequency of the impactor was gradually increased during each cycle from 6 to 11 Hz, with stepped increments of 1 Hz. The grinding programme was suggested based on previous experience with grinding of a wide range of different types of matter, and was expected to offer maximal disintegration effect. [16] [17]. The structural characterization of the S powders as well as printed cathodes was carried out by a field-emission scanning electron microscope (FE-SEM, JEOL JSM 7500F).

Dimensions of the particles in S powders were measured and statistically analyzed by NanoMeasure software. Average values (n = 200 for each type of powder) and standard deviations were calculated for all the measurements performed. X-ray diffraction analyses were also carried out using X-ray diffractometer (D8 Advance, Bruker, Cu Kα radiation, step 0.02 2theta).

2.2. Cell assembly and testing

Two slurries were prepared for the fabrication of the cathodes. If not denoted otherwise, all chemicals for the slurries were purchased from Sigma Aldrich. The first slurry based on the reference S powder consisted of an S (milled in a planetary ball mill at 500 rpm for 30 min), carbon Super P, and poly(vinylidenefluoride) (PVDF) in the weight ratios of 80:10:10 or 60:30:10, respectively, dispersed in N-Methyl-2-pyrrolidone (NMP). These cathodes are further noted in text as S_{ref60} or S_{ref80} cathode, depending on the S content. The slurry was deposited onto Al foil, after 24 hours of stirring by a coating bar, and subsequently dried in an oven at 60 °C for 24 hours. The prepared layer was then pressed by the pressure of 500 kg/cm². Afterwards, discs with the diameter of 18 mm were cut out of all pressed layers, dried again in a vacuum, transferred to a glove box (under Ar atmosphere,) and finally dried in an oven at 60 °C. The second slurry consisted of cryo-ground S powder (stored previously in a freezer at -18 °C), carbon Super P and PVDF in the weight ratio of 80:10:10, respectively, all dispersed in NMP. Mixing was carried out while cooling in an ice bath with a temperature below 0 °C. After 24 hours of stirring using a magnetic stirrer, the slurry was deposited by a coating bar onto Al foil, and dried in vacuum at 20 °C for 24 hours. The prepared layer was then pressed by the pressure of 500 kg cm⁻². Afterwards, discs with the diameter of 18 mm were cut out of all pressed layers, and stored in a fridge at 5 °C inside a glove box. This cathode is further noted in text as S_{cryo} cathode.

All cathode layers were inserted into the electrochemical test cell ECC-STD (El-Cell©). The whole assembly was done in the glove box. Metallic Li was used as a counter electrode, and 0.25 M of lithium nitrate ($LiNO_3$) + 0.7 M of lithium bis(tri-fluoromethanesulfonyl)imide (LiTFSI) solution, in 1,2-dimethoxyethane (DME) and 1,3-dioxolane (DOL) was used as an electrolyte, where the ratio was: DME:DOL 2:1 v/v. The electrolyte was impregnated in a glass fiber based separator.

Cyclic voltammetry (CV) and galvanostatic cycling were used for electrochemical characterization using VMP3 potentiostat (Bio-logic). CV curves were recorded in the potential window from 1.0 to 3.4 $V_{vs.\ Li}$, and the scan rate was set to 0.1 mV s^{-1}. Galvanostatic cycling was carried out within a potential window from 1.5 to 3.0 $V_{vs.\ Li}$. All measurements were performed at 20 °C. SEM and XRD analyses were carried out in the same manner as for the S powders, as previously described in section 2.1

3. Results and discussion

Figure 1a shows a photograph of the initial crystalline S piece that was subsequently melt-quenched and converted into an amorphous glassy S – an illustrative photograph of this glass structure is shown in Figure 1b. Immediately after the melt-quenching, the amorphous glass S piece was placed into liquid N_2 and transported to the cryogenic grinder for grinding. Figures 1c and 1d show resulting cryo-ground S particles at two different magnifications. From the low magnification SEM image of the cryo-ground S powder (Fig. 1c), one can see particles with relatively broad range sizes. Particles have many edges and rather irregular shapes, as shown in detail in Fig. 1d. In contrast, particles of reference S powder shown in display comparably narrower range of sizes (Fig. 1e), and very round particle shapes (Fig. 1f). The average measured (SEM derived) dimensions of the particles were 9.2±2.4 μm, and 6.7±1.5 μm for the cryo-ground and reference S powders, respectively. It has to be noted that for the

purpose of SEM and XRD investigation, the S cryo-ground powder had to be exposed to laboratory temperature, in contrast to the cathode preparation, which was carried out at -18°C. Thus, the S cryo-ground powder was already crystallized from its initial state before these analyses were carried out. This is also seen from Figure 1g that shows the comparison of XRD data for both powders. Clearly, both diffractograms are nearly identical, and display orthorhombic S structure (alpha-S_8 – space group: Fddd). Conversion of the amorphous cryo-ground powder into crystalline one will be discussed later.
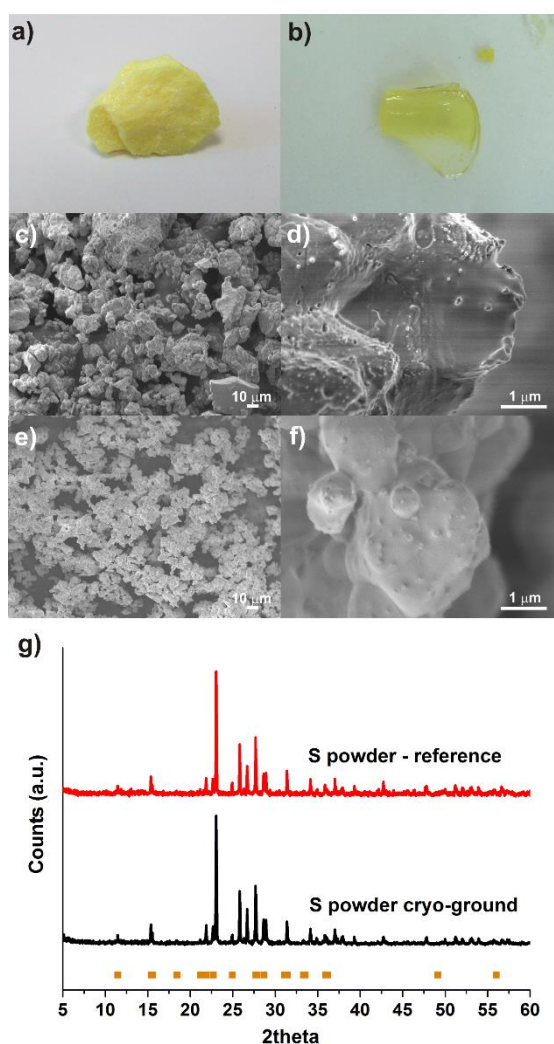

Fig. 1: (a) photograph of crystalline S piece before melt-quenching, (b) photograph of amorphous glassy S before cryogenic grinding; SEM images cryo-ground (a, b) and reference (c, d) S powders used for the cathode in this work; (g) comparison of X-ray diffractograms for

both powders showing orthorombic S structure. The symbols in (g) show XRD line positions of orthorhombic (Fddd) S.

Figure 2a shows CV curves recorded with the scan rate of 0.1 mV s^{-1} within the 1st and 3rd cycle for both S-based cathodes, based on powders shown in Figure 1. The CV curves display currents related to either mass, provided that both slurries used for this comparison contained equal amount of S powders (80 wt. %). In all cases, two cathodic peaks at 2.0 and 2.4 V were recorded. The 2.4 V peak corresponds to the reduction of elemental S to higher-order lithium polysulfides, and their subsequent reduction (2.0 V peak) to lower-order lithium polysulfides. [18] [19] Both cathodic peaks for S_{cryo} cathode are lower in all cases. On the other hand, as evident from Fig. 2a, the S_{ref80} cathode showed a higher activity than the S_{cryo} cathode only within the 1st cycle, whereas it decreased with an increasing number of cycles. This is particularly evident from Fig.2b, which shows the stability of capacities and Coulombic efficiencies for both cathodes within 50 cycles. As one can see, the performance of S_{cryo} cathode was significantly more stable in comparison with S_{ref80} cathode, whose capacity dropped down significantly upon cycling. On the other hand, the Coulombic efficiency did not considerably increase due to strongly decreasing ratio between supplied charge and obtained charge during one cycle. All in all, this is an exciting result, as the literature reports significant decline of capacity for cathodes based on S contents higher than 70 wt.%. [14] [20] However, even with the 80 wt. % content of S in the slurry, the cryo-ground S powder seems to have increased stability against unwanted reduction into polysulfides than the reference S powder, which is evident from rather broad and rounded cathodic peaks of the S_{cryo} cathode, seen in Fig. 2a.
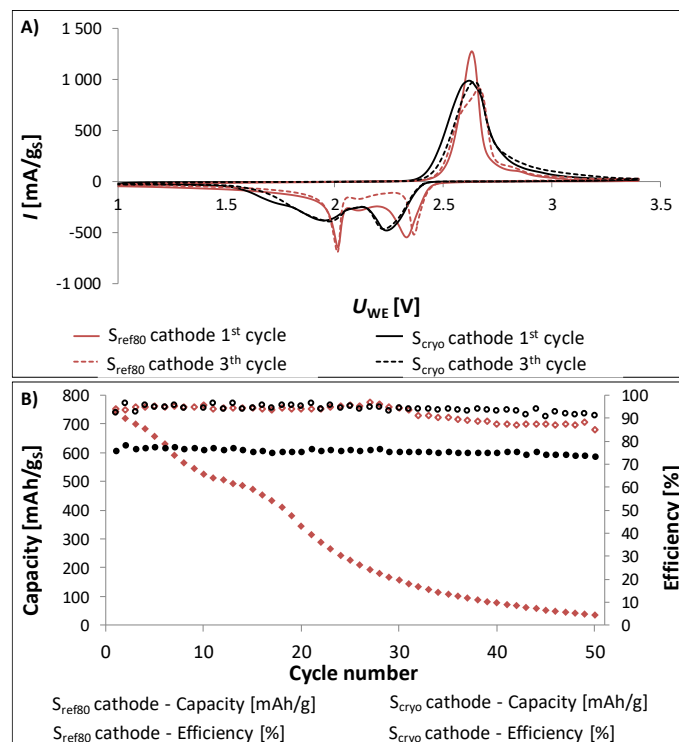
Fig. 2: a) CV curves recorded for the cathodes based on 80 wt.% content of cryo-ground S powder (marked S$_{cryo}$ cathode), or reference S powder (marked S$_{ref80}$ cathode) during the 1st and 3rd cycle, at the scan rate of 0.1 mV s^{-1}; b) performance stability of both cathodes upon 50 cycles at 0.2 C displayed as capacity (mAh.$_g$S^{-1}) and Coulobmic efficiency (is determined by the ratio between the supplied charge and obtained charge during one cycle)

In order to overcome the low stability of the S reference powder, succeeding slurries contained a lower content for reference in the subsequent charging/discharging tests. Figure 3a,b shows CV curves obtained similarly as in Figure 2, with the exception that the curve for the reference S-based cathodes was produced with a slurry of lower S content (60 wt. % from 80% shown in Fig.2). Again, two cathodic peaks at 2.4 and 2.0 V were recorded that correspond to the reduction of elemental S to higher-order Li-polysulfides, and their subsequent reduction to lower-order Li-polysulfides. However, in this case, both of the cathodic peaks were comparable within the 3rd cycle for both cathodes, which was due to the lower S content, and less pronounced reduction into polysulphides. In this case, we provided CV curves expressed as per unit of S loading (Fig. 3a) as well as per unit of cathode area (Fig. 3b). This in order to emphasize the difference in the S loading within each cathode layer and

to underline the fact that even with higher sulphur loading in the case of of S_{cryo} cathode (80%), better results can be achieved thanks to the correct composition and proper utilization of the cathode.
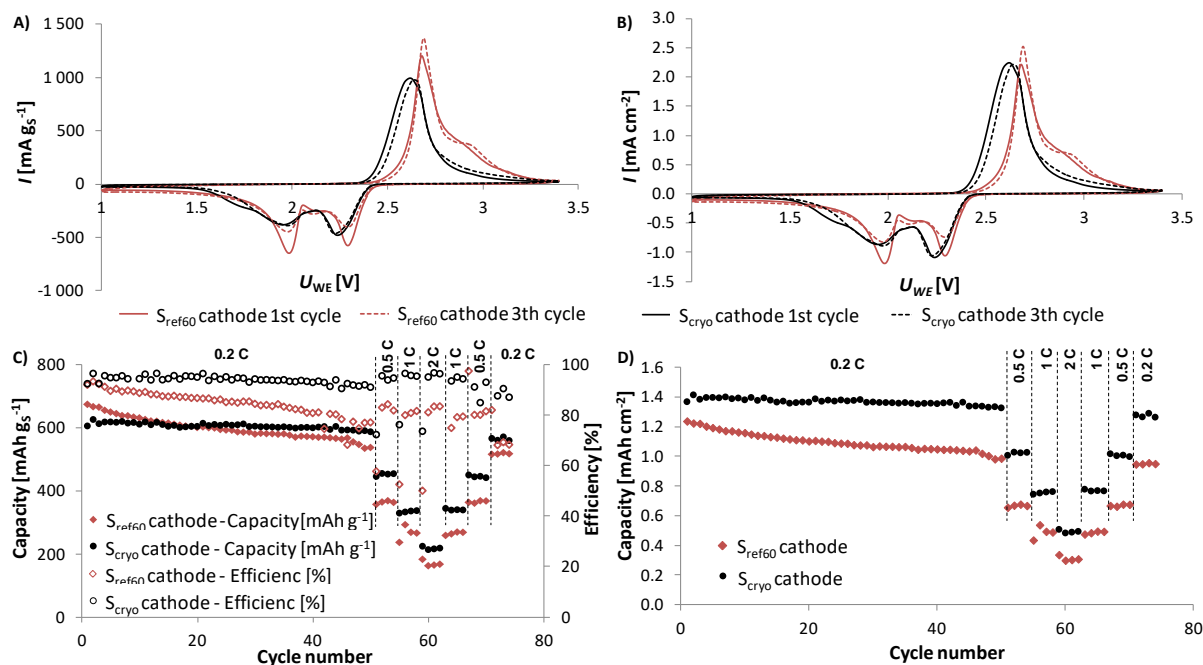

Fig. 3: a) CV curves recorded for S_{cryo} cathode (based on cryo-ground S powder, 80 wt.% content) or S_{ref60} cathode (based on reference S powder, 60 wt.% content) during the 1st and 3th cycle at the scan rate of 0.1 mV s^{-1}; per gram of S; b) the same curves as in a), but per cm^2 of cathode; c) Performance of both cathodes expressed as the change of capacity per gram of S and the Coulombic efficiency during cycling at different C- rates (based on the S loading); d) same curves as in c) but per cm^2.

Figure 3c, d shows the performance of both cathodes in terms of the charge capacity and the Coulombic efficiency, recorded using over 80 cycles at different C-rates. Besides the low S content (60 wt.%), the diminished capacity for the S_{ref60} cathode was more pronounced compared to the S_{cryo} cathode. As one can see, the capacity as well as the Coulombic efficiency, were higher for the S_{cryo} cathode (except the first approximately 20 cycles), regardless of the C-rate used for the charging. In addition, when expressed as the capacity per gram in Figure 3d, the performance of the S_{cryo} cathode was outstanding. These results clearly

suggest that the performance of both cathodes will be significantly different, especially with a high number of cycles passed.

In order to obtain a deeper insight of the performance stability, galvanostatic cycling at various C-rates was carried out for both cathodes. Figure 4 shows the capacity retention during galvanostatic cycling at various C-rates.

Initially, the results for the first 50 discharging cycles at 0.2 C are shown in Figure 4a and b for the S_{ref60} and S_{cryo} cathodes. As one can see, the S_{ref60} cathode (Fig. 4a) starts cycling at 0.2 C with a higher capacity (674.6 mAh g^{-1}) than the S_{cryo} cathode (606.1 mAh g^{-1}). However, it loses its capacity with the increasing number of cycles.Its capacity after 50 cycles decreased to 537.7 mAh g^{-1}, which accounts for $\approx$ 20.3% of the capacity loss. This loss is also apparent from the overall comparison shown in Fig. 3c and d (see first 50 cycles). It is noteworthy, that the capacity loss of S_{ref60} is significantly smaller compared to S_{ref80} cathode (see data for S_{ref80} Fig. 2b), where the instability of S (volumetric expansion, pronounced polysulfide formation) came into play leading to much more pronounced capacity loss.

Moreover, it is evident from Figure 3c, that its Coulombic efficiency also decreased from the initial value of 92% to 77%. Contrastingly, the S_{cryo} cathode (Fig. 4b) exhibited comparably higher stability during the first 50 cycles at 0.2 C, with the capacity around 600 mAh g^{-1}. Its capacity in the last cycle was 587.7 mAh g^{-1}, which accounts only for $\approx$ 3% of the capacity loss. In addition, as evident from Figure 3c, its Coulombic efficiency remained very high - between 95% and 92%.
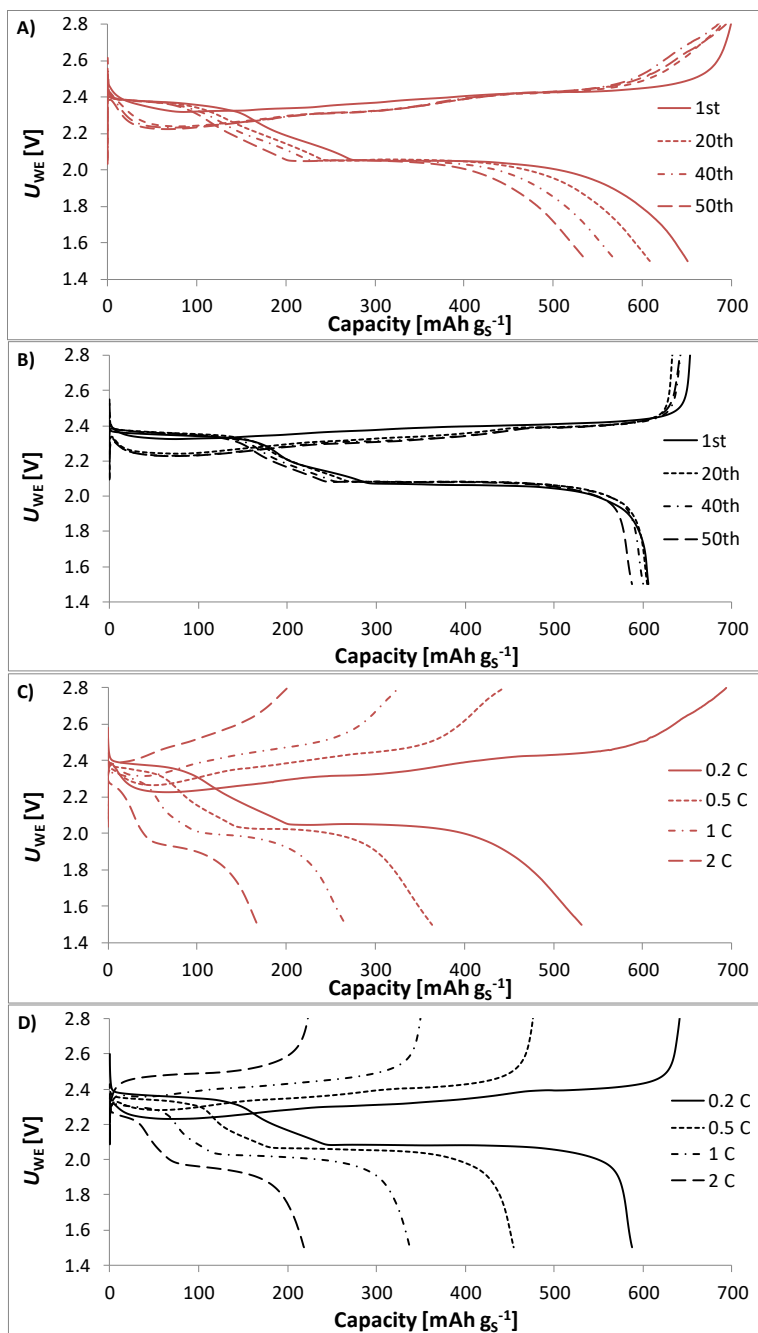
Fig. 4: Comparison of discharge curves for a) S_{ref60} cathode and b) S_{cryo} cathode, recorded during the first 50 cycles at 0.2C. Comparison of charge/discharge curves for: c) S_{ref60} cathode and d) S_{cryo} cathode at different C-rates. The upper curves represent charging, whilst the lower curves discharging. Data was taken from the last cycle of the corresponding C-rate.

Figure 4c and d shows the capacities recorded in the subsequent cycling at higher loads, where capacities for S_{cryo} cathode (Figure 4d) at all C-rates were higher compared to the S_{ref60} cathode (Figure 4c). For example, the last (50th) cycle produced values of 454.8 mAh g^{-1} vs. 363.7 mAh g^{-1}, respectively, at 0.5 C, and values of 218.8 mAh g^{-1} vs. 167.8 mAh g^{-1},

respectively, in the last (50th) cycle at 2C. The total drop of capacity during the whole cycling decreased by 7.6 % and 23.2 %, respectively. The efficiencies at the end of cycling (not shown in Figure 4) were maintained at 87.5 % vs. 68.3 % respectively.

Finally, upon comparison of the charging and discharging curves in Figure 4, one sees a large difference between both cathodes. When considering the charging curves, the S_{cryo} cathode maintains a stable charging plateau at 2.4 V, at higher capacities compared to S_{ref60} cathode, for which there is no stable plateau at 2.4 V, under any load. When considering the discharging curves, there are some plateaus at 2.0 V achieved for the S_{ref} cathode (in contrast to charging), however, the S_{cryo} cathode displays considerably larger capacities even under the load of 2 C.

In order to explore the reasons behind the enhanced performance of S_{cryo} over S_{ref60} cathodes, a detailed inspection of prepared cathodes was carried out by SEM (in particular by cross-sectioning), EDX and XRD. Figure 5 shows result of this inspection. Both layers had a similar thickness: 17±2 μm and 21±2 μm for S_{cryo} over $S_{ref60,}$ respectively. However, on the first look, the confinement of S particles within the cathodes was very different. For S_{ref60} layers, the size and shape of S particles remained similar to the starting material. In contrast, the S cryo-ground particles within S_{cryo} cathodes were found to be approximately 3-4 times smaller (approx. 2-3 μm) compared to their nominal size (approx. 9.2 μm) before entering into the cathode slurry. This size decrease was also confirmed by EDX mapping measurements (not shown), which revealed a considerably large density of small S regions within the S_{cryo} cathode layer, compared to considerably smaller density of larger S regions within S_{ref60} cathode layer. Figure 5e shows comparison of XRD patterns recorded from both cathode layers (S_{cryo} vs. S_{ref60}) after their preparation. The average crystallite size was evaluated from the Scherrer equation as 61 nm and 67 nm, for the S_{cryo} cathode and S_{ref60} cathode. Similar as in Figure 1g, S was within the cathode layers present in the orthorhombic state. However, in

the case of S$_{cryo}$, the XRD pattern resembles more or less the same pattern shown in Figure 1g for the cryo-ground S powder. This means that the cryo-ground S powder within the cathode did not undergo any obvious change in the crystallinity. In contrast, there is apparent change in preferential crystal orientation between reference S powder (Figure 1g) and the S within the S$_{ref60}$ cathode (Figure 5e). Reasons for this difference remain unclear at this stage and will be subject of further investigation.
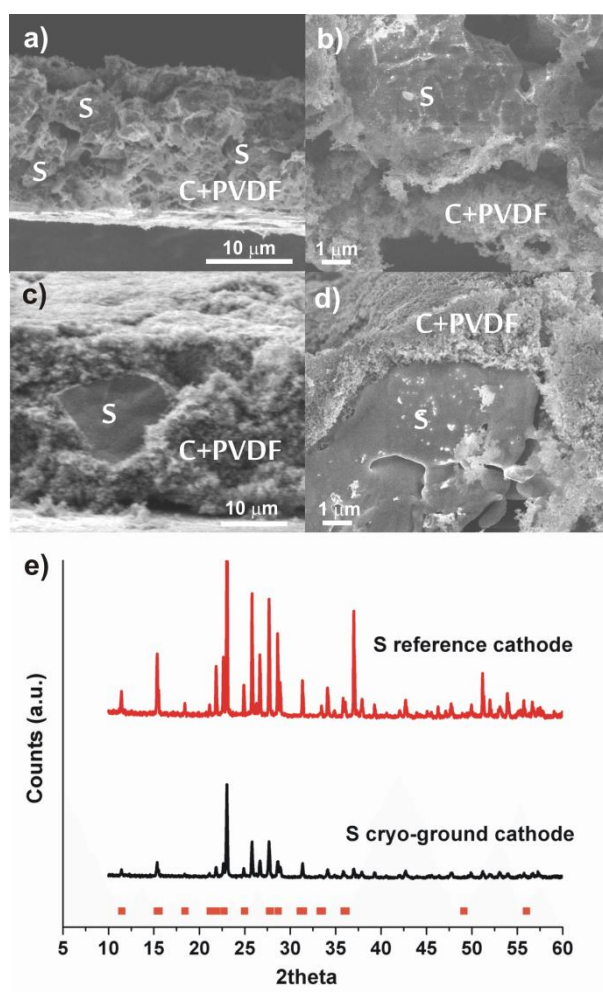

Fig. 5: SEM cross-sectional images of S$_{cryo}$ (a,b) and S$_{ref60}$ (c, d) cathode layers after their preparation shown in different magnifications. Symbols (S, C, PVDF) indicate particular composition at the given spot (derived from EDX mapping); (e) comparison of X-ray diffractograms of identical cathode layers as in (a-d) showing orthorombic S structure. The symbols in (e) show XRD line positions of orthorhombic (Fddd) S.

It is hypothesized that the decrease of the diameter of cryo-ground S particles from the cryo-mill to the cathode layer can be due to either their additional breaking during the cathode

preparation (which was possible due to their complete or at least partial amorphicity when entering the slurry) or by de-agglomeration in the highly dispersive environment of the slurry, (i.e. the particles shown in Figure 1c and d were still agglomerates of smaller particles), or by combination of both factors. Let us discuss first the particle´s breaking during the cathode preparation. We speculate that the further crystallization in the slurry leading to the structural changes (where S-chains are replaced by S_8 rings [21]) as well as a density difference between the amorphous and crystalline states (approx. 8% [22]) might have induced an additional impact on the cryo-ground S particles to fall apart during the cathode preparation. In other words, in contrast to crystalline reference S particles, cryo-ground S particles were entering the cathode slurry in the amorphous state under cryostatic conditions (-18 °C). This temperature is on one hand slightly above the glass transition temperature (T_g of S ≈ -30 °C [23]), thus the phase-transition of S from the true glassy state to the crystalline state proceeded rather reluctantly. Even though the cryo-ground S particles must have crystallized in the cathode layer at some point (at latest by the time of XRD measurement several days after synthesis at ambient laboratory temperature, as shown in Figure 1g), apparently, there was some period during which particles remained in the cathode slurry still amorphous and could undergo further size decrease by slurry mixing, as revealed by SEM and EDX inspections.

The second possibility - the size decrease of cryo-ground S particles due to de-agglomeration of aggregated particles in highly dispersive environment of the cathode slurry - is plausible too. However, even upon extensive SEM analyses of cryo-ground S particles at various magnifications, it was not possible to identify agglomerates. Thus the cryo-ground S particles shown in Figure 1c and d were thus still considered (and discussed within this paper) as rather single particles, then agglomerates. However, the presence of agglomerates cannot be completely neglected due to the specific impact of the cryogenic grinding on resulting ground

particles. Other techniques, apart SEM, such as dynamic light scattering (DLS) or transmission electron microscopy (TEM) failed in this case. The DLS could not distinguish, whether the particles were agglomerates or not, especially if there was a very tight interconnection. For TEM the particles were simply too large to be penetrated by electrons.

Nevertheless, the better performance of S_{cryo} cathode can be ascribed to better confinement of the cryo-ground S powder in the resulting cathode layer due to a specific shape (and smaller size) of particles given by cryogenic grinding. The resulting S_{cryo} cathode layer shows denser packing of S with other cathode consituents (i.e. C+PVDF) and therefore also possesses fewer voids.

In all cases, polysulfides are created during the cycling, as apparent from Figure 2, 3 and 4. However, it seems as if the dissolution of S into polysulfides is less pronounced in the case of S_{cryo} in comparison with S_{ref}. It is likely due to better packing of S powder with C and PDVF binder within the S_{cryo} cathode layer, which is in line with observations in Figure 5. In fact, as we observed higher capacities at higher C-rates for the S_{cryo} cathode, it means that this layer has higher intrinsic conductivity compared to the S_{ref60} layer, besides a considerably lower content of conductive C particles in the slurry (i.e. 30 wt.% in S_{ref60} cathode vs. 10 wt.% in S_{cryo} cathode). Apparently, there is an improved percolation between C and S particles in the case of S_{cryo} powder. As a result, the overall performance of the S_{cryo} cathode is improved. A detailed investigation of this aspect will be subject of our further work.

4. Conclusions

Performance of cathode layers (S_{cryo}) containing sulfur powder prepared by cryogenic grinding of bulk S, were compared to cathode layers based on reference S powder (S_{ref60}). S_{cryo} cathodes exhibited extraordinarily high stability during cycling, despite of higher sulfur loading (80 % of the mass of electrode, 2.26 mg cm^{-2}), in combination with carbon and basic

PVDF binder. The cathode type reached a higher efficiency, stability and a higher capacity at high C-rates in comparison with the standard S_{ref60} cathode. Despite the fact that cryo-ground powder crystallized in the cathode layer, utilization of cryo-ground amorphous powder for the preparation of cathodes, even at very high content (80 wt. %), resulted in a favorable confinement of S within the layers that restricted the dissolution of polysulfides in the electrolyte, and improved the efficiency of cycling in this work. This approach can potentially solve the stability of cathodes, which is one of the current challenges of Li-S batteries.

Acknowledgement

References

[1]   B. Scrosati, History of lithium batteries, Journal of Solid State Electrochemistry. vol. 15 (2011).

[2]   Y. Yin, S. Xin, Y. Guo, L. Wan, Materials, and Prospects, Angewandte Chemie International Edition. vol. 52 (2013).

[3]   H. Yoo, E. Markevich, G. Salitra, D. Sharon, D. Aurbach, Materials Today. vol. 17 (2014).

[4]   R. Brodd, Batteries for sustainability: selected entries from the Encyclopedia of sustainability science and technology, Springer-Verlag New York, New York, 2013.

[5]   J. Kim, D. Lee, H. Jung, Y. Sun, J. Hassoun, B. Scrosati, Advanced Functional Materials. vol. 23 (2013).

[6]   P. Bruce, S. Freunberger, L. Hardwick, J. Tarascon, Nature Materials. vol. 11 (2011).

[7]   G. Babu, K. Ababtain, K. Ng, L. Arava, Scientific Reports. vol. 5 (2015).

[8]   A. Fedorková, R. Oriňáková, O. Čech, M. Sedlaříková, International Journal of Electrochemical Science. vol. 8 (2013).

[9]   J. He, Y. Chen, P. Li, F. Fu, Z. Wang, W. Zhang, J. Mater. Chem. A. vol. 3 (2015).

[10] X. Zhao, J. Tu, Y. Lu, J. Cai, Y. Zhang, X. Wang, C. Gu, Electrochimica Acta. vol. 113 (2013).

[11] J. Wang, Y. Yang, F. Kang, Electrochimica Acta. vol. 168 (2015).

[12] X. Wang, Z. Zhang, X. Yan, Y. Qu, Y. Lai, J. Li, Electrochimica Acta. vol. 155 (2015).

[13] L. Xiao, Y. Cao, J. Xiao, B. Schwenzer, M. Engelhard, L. Saraf, Z. Nie, G. Exarhos, J. Liu, Advanced Materials. vol. 24 (2012).

[14] H. Yao, K. Yan, W. Li, G. Zheng, D. Kong, Z. Seh, V. Narasimhan, Z. Liang, Y. Cui, Energy Environ. Sci. vol. 7 (2014).

[15] K. Dokko, N. Tachikawa, K. Yamauchi, M. Tsuchiya, A. Yamazaki, E. Takashima, J. Park, K. Ueno, S. Seki, N. Serizawa, M. Watanabe, Journal of the Electrochemical Society. vol. 160 (2013).

[16] P. Knotek, M. Pouzar, M. Buzgo, B. Krizkova, M. Vlcek, A. Mickova, M. Plencner, J. Navesnik, E. Amler, P. Belina, Materials Science and Engineering: C, 32 (2012).

[17] M. Pouzar, A. Krejcova, T. Cernohorsky, K. Peskova, Talanta, vol. 76 (2008).

[18] M. Rao, W. Li, E. Cairns, Electrochemistry Communications. vol. 17 (2012).

[19] J. Guo, Y. Xu, C. Wang, Nano Letters. vol. 11 (2011).

[20] M. Hagen, S. Dörfler, P. Fanz, T. Berger, R. Speck, J. Tübke, H. Althues, M. Hoffmann, C. Scherr, S. Kaskel, Journal of Power Sources. vol. 224 (2013).

[21] K. Andrikopoulos, A. Kalampounias, S. Yannopoulos, Soft Matter. 7 (2011).

[22] J. Borsboom, J.A. Lagas, Process for removing elemental sulfur from a gas stream, 1998.

[23] A. Tobolsky, W. MacKnight, R. Beevers, V. Gupta, Polymer. 4 (1963).